Augmented Reality User Interface for an Atomic Force Microscope based Nanorobotic System

Wolfgang Vogl, Bernice Kai-Lam Ma, and Metin Sitti, *Member, IEEE*

***Abstract*—A real-time augmented reality (AR) user interface for nanoscale interaction and manipulation applications using an atomic force microscope (AFM) is presented in this paper. Nanoscale three-dimensional (3D) topography and force information sensed by an AFM probe are fed back to a user through a simulated AR system. The sample surface is modeled with a B-spline based geometry model, upon which a collision detection algorithm determines, whether and how the spherical AFM tip penetrates the surface. Based on these results, the induced surface deformations are simulated using continuum micro/nanoforce and Maugis-Dugdale elastic contact mechanics models and 3D decoupled force feedback information is obtained in real-time. The simulated information is then blended in real-time with the force measurements of the AFM in an AR human machine interface, comprising a computer graphics environment and a haptic interface. Accuracy, usability, and reliability of the proposed AR user interface is tested by experiments for three tasks: positioning the AFM probe tip close to a surface, just in contact with a surface, or below a surface by elastically indenting. Results of these tests showed the performance of the proposed user interface. This user interface would be critical for many nanorobotic applications in biotechnology, nanodevice prototyping, and nanotechnology education.**

***Index Terms*—Telenanorobotics, Augmented Reality user interfaces, nanomanipulation, Atomic Force Microscopy**

I. Introduction

ATOMIC force microscopes (AFM) are tactile imaging instruments with a resolution down to atomic scale. Probing the sample surface with a nanoscale scanning tip attached to a compliant cantilever, three-dimensional (3D) topography of a surface and also its tribological properties can be obtained by detecting the deflection and twisting of the cantilever using a laser beam. Typical scanning tip apex radii are around 10 nm and the positioning resolution of the tip is on the range of some hundred picometers. Measuring the deflection of the cantilever, forces exerted on the tip can be sensed with a resolution down to piconewtons.

Beginning with a pioneering work in 1990 [1], AFMs or other scanning probe microscopes have been employed not only for imaging, but also as teleoperated manipulators at the micro- and nanoscale. The AFM probe is controlled in a suitably scaled way by a haptic master device on which the user can feel the forces interacting between scanning tip and sample surface. Comprising also a 3D computer graphics environment, which displays a previously scanned image of the sample surface and the current position of the AFM probe tip, these systems provide a highly intuitive way of interaction with objects at the nanoscale. They can be considered as teleoperation user interfaces for nanomanipulation, where teleoperation is employed to bridge a huge difference in scale, rather than in distance.

A great variety of telenanorobotic systems has been introduced over the recent decade. A wide range of haptic devices has been employed for telenanorobotics ranging from a magnetic levitation device with 6 degrees of freedom (DOF) [1], a force-reflecting 1-DOF device [2,3], Phantom™ [4-6] or the Delta™ haptic device [7] with 3-DOF, and even a force-feedback game joystick [8]. Example nanomanipulation applications include nanoscale particle pushing [9-11], chromosomal dissection [12], and cell manipulation [5]. One of the first AFM user interface systems [13] is now even available as a commercial product.

In these works, it has been agreed that modeling the physics of the interaction between tip and sample is necessary to realize complicated tasks like manipulation of objects [4,7,9,14], but also to enhance the quality of the user interface [3,7,15]. Here, the design of AFMs puts two crucial constraints to these user interfaces in ambient conditions, which both decrease the intuitiveness of interaction:

- *No on-line visual feedback*: Deformations induced by the AFM probe and real-time AFM tip and nanoobject positions cannot be seen. Only an off-line previously scanned image of the surface is shown to the user as no imaging is possible in ambient conditions while the tip is employed in manipulation. However, scanning electron microscope can enable real-time nanoscale imaging in vacuum conditions which is out of domain of this work.
- *No 3D decoupled force measurement*: The force sensing of AFM cannot resolve the force interacting between the scanning tip and the probed surface in three dimensions independently. As can be seen in Figure 1, $\Delta\alpha$ deflection

Manuscript received April 1, 2005.

Wolfgang Vogl is with the IWB-Institute for Machine Tools and Industrial Management, Technical University of Munich, Munich, Germany (e-mail: wolfgang.vogl@iwb.tum.de).

Bernice Kai-Lam Ma was with Carnegie Mellon University, Computer Science Department, Pittsburgh, PA 15213 USA (e-mail: bkm@andrew.cmu.edu).

Metin Sitti is with the NanoRobotics Laboratory, Mechanical Engineering Department and Robotics Institute, Carnegie Mellon University, Pittsburgh, PA 15213 USA (phone: 412-268-3632; fax: 412-268-3348; e-mail: sitti@cmu.edu).

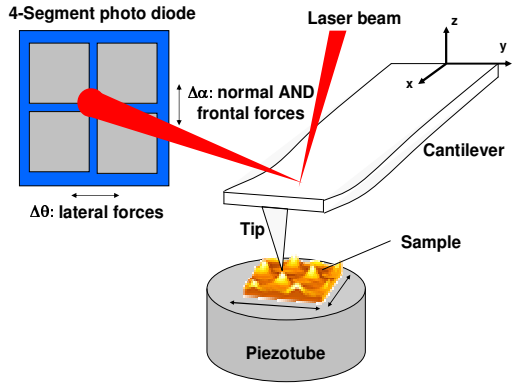

Figure 1. AFM force sensing: frontal and normal forces are measured in a coupled way, while lateral forces are measured separately. Therefore, decoupled 3D-force feedback is not possible.

is due to both frontal forces in *x*-direction and normal forces in *z*-direction.

These limitations are inherent in the design of AFM based nanorobotic systems and cannot be overcome easily. On-line visual feedback could be provided using a hybrid approach with a scanning electron microscope (SEM) [16], but this again introduces new complications such as limiting the nanorobotic applications to vacuum environments and handling only conductive or semiconductive materials. Exact force feedback and position control could be gained by limiting the directions of movement to two dimensions (*y*- and *z*-directions in Figure 1), however for a random 3D nanomanipulation application 3D decoupled force feedback is required [6].

In this paper, for the first time, a *real-time* physical simulation of nanoscale surface interactions is displayed by integrating B-spline based 3D computer graphics techniques with continuum nanoforce models for non-contact and contact interactions. Furthermore, a scheme of decoupling 3D forces in an AFM is proposed for reliable force feedback. Accuracy, usability, and reliability of the proposed AR user interface are tested by experiments for three specific tasks. Here, although real AFM images are used to simulate force and visual feedback, the system is not currently connected to an experimental AFM system. This type of user interface would be critical for many nanorobotic manipulation and interaction applications for animated real-time 3D visualization, 3D decoupled force feedback, and intuitive teleoperation.

II. Augmenting Measured with Modeled Information

In this work, models have been developed to model lacking information, i.e. surface deformations and 3D resolution of forces exerted on the tip. This information is simulated and blended in real-time with the information sensed by the AFM probe in an augmented reality (AR) user interface as shown in Figure 2. This way, the interaction with the user interface can be enhanced concerning haptic as well as also visual feedback. Combining simulation results and measured information, decoupled 3D force feedback from the AFM probe can be given to the user and otherwise invisible deformations can be visualized in real-time. The following information is modeled

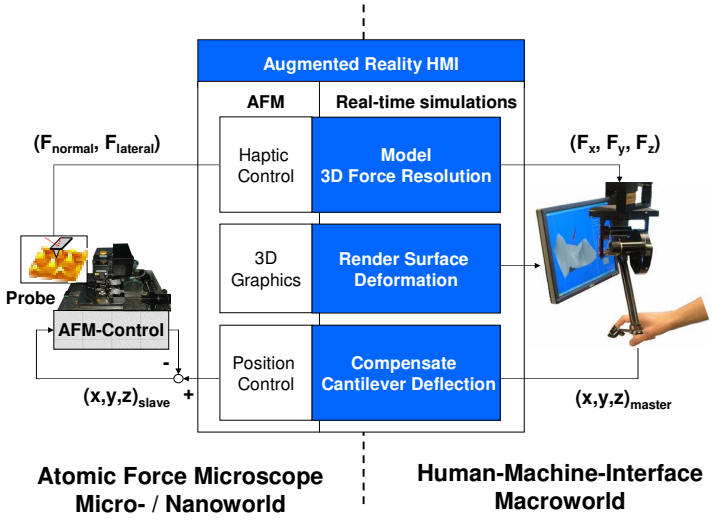

Figure 2. System concept: Sensed and simulated information are blended in real-time.

as it cannot be determined from the AFM directly during teleoperated nanomanipulation:

- Deformed shape of the sample surface in contact with the spherical scanning tip,
- Geometry of contact, respectively the normal direction of the contact between the arbitrarily shaped sample surface and the spherical AFM tip.

The deformation of the surface and also the deformation of the cantilever can then be displayed to the user during the telemanipulation as proposed in [3]. Using the geometry of the contact and the cantilever deformation model, the two measured force signals can be decoupled into 3D force feedback. Also the deflection of the tip from its position at zero force is obtained in 3D and can be used for position control.

III. Spline Based Surface Model

A spline based representation through the widely used and also OpenGL supported B-splines is chosen for geometrical representation of the sample surface. A previously scanned image of the sample surface is first smoothened with a Gaussian low-pass filter to remove noise and then a bicubic B-Spline surface is fitted onto the data points. This way, a continuous, parametric 3D representation $\boldsymbol{S}(u,v)$ of the sample surface is obtained. During the teleoperation, a collision detection algorithm checks for collisions between the spline surface and the spherical AFM tip. In case of collisions, the spline is deformed by control point repositioning to visualize the deformation induced by the tip.

A. Collision Detection

Detecting collisions between the spline representing the sample surface and a sphere representing the AFM tip as displayed in Figure 3 can be realized by orthogonal projection of the tips center onto the spline. Projecting a point $\boldsymbol{C}$ onto the spline surface $\boldsymbol{S}(u,v)$ corresponds to finding the shortest distance between $\boldsymbol{C}$ and a point of the spline. The vector

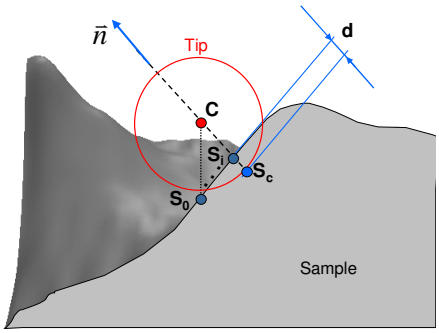

Figure 3. Collision detection yields normal direction *n* and indentation depth *d*.

function $\boldsymbol{r}(u,v)$ describes the vector between a point $\boldsymbol{S}(u,v)$ on the spline surface and a point $\boldsymbol{C}$:

$$\mathbf{r}(u,v) = \mathbf{S}(u,v) - \mathbf{C}. \tag{1}$$

The following two scalar equations are held when $\boldsymbol{r}$ is perpendicular to the spline surface, respectively when the distance between $\boldsymbol{C}$ and $\boldsymbol{S}$ is minimized:

$$\begin{aligned} f(u,v) &= \mathbf{r}(u,v)\cdot\mathbf{S}_u(u,v) = 0, \\ g(u,v) &= \mathbf{r}(u,v)\cdot\mathbf{S}_v(u,v) = 0. \end{aligned} \tag{2}$$

Solving this equation system for the two unknown u and v can be done using binary search on the spline parameters u and v like in [17]. This approach has the advantage that binary search always converges after a defined number of steps. Yet, it is only guaranteed to work for convex surfaces and may lead to errors for concave ones. We therefore chose the Newton-Raphson method, which works also for concave surfaces, to solve the above equations as described in [18].

As convergence is not guaranteed, additional starting guesses are selected in the case that the algorithm does not converge. The following double iterative scheme gives good convergence for a broad range of surfaces:

1. Try last solution as the start value if algorithm does not converge.
2. Project $\boldsymbol{C}$ onto $\boldsymbol{S}$ along the z-axis yielding $\boldsymbol{S_0}$ and use the obtained parameter pair (u_0,v_0) as start values, if algorithm does not converge.
3. Repeatedly try points in proximity of $\boldsymbol{S_0}$ until a solution is found.

The collision detection algorithm yields the point $\boldsymbol{S_i}$ closest to the center $\boldsymbol{C}$ of the spherical tip, and also the normal direction $\vec{n}$ of the interaction between tip and surface and the indentation depth d, with which the tip penetrates the surface.

B. Surface Deformation Modeling

In order to visualize the deformation of the sample surface, the control points of the spline are repositioned in case of contact. A copy of the spline used for collision detection is first altered and then rendered using OpenGL's NURBS implementation. Two different repositioning schemes are possible:

- Repositioning only 4 control points, moving $\boldsymbol{S_i}$ exactly as far as the indentation depth d along the contact direction $\vec{n}$ (i.e. to the predicted contact point $\boldsymbol{S_c}$),
- Repositioning all control points in the area of contact such that the spline conforms to the spherical shape of the AFM tip.

The first approach was chosen by [17] and can be found in [18]. It gives visually acceptable results for smaller indentation depths and is computationally less expensive. However for greater indentation depths, it gives visually disturbing results.

The second approach which repositions all control points in the area of contact is mainly used in this work. All control points in the area of contact, i.e. points which lie within the contact radius, are projected onto the sphere representing the tip as shown in Figure 4. Here, contact radius, a, is determined by the Maugis-Dugdale elastic contact mechanics model [3] which is the most accurate continuum micro/nano-contact mechanics model for AFM studies. As a B-spline always lies in the convex hull of its control polygon, the shape of the surface approximately conforms to the spherical shape of the tip in the area of contact. This approach gives a visually good approximation for the shape of the deformed surface sufficiently many control points are repositioned. This way, both indentations and adhesion effects of the sample surface can be visualized when the tip sticks to the sample.

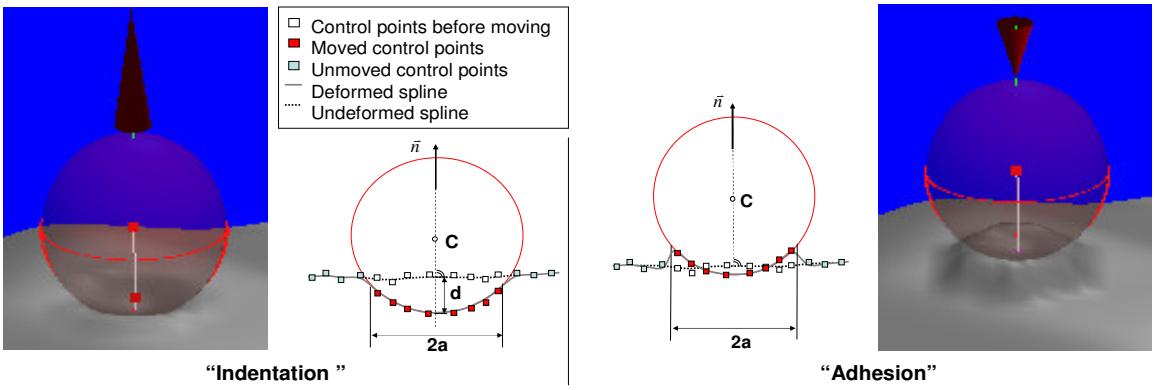

Figure 4. Screenshots and schematics of surface deformation: the interaction between tip and surface can be visualized to the user in 3D (the sphere and cone represents the AFM tip and forces acting on the tip, respectively). The left two images show the *indentation* (elastic deformation) of the surface and repulsive contact forces while pressing to the surface, and the right two images show the *adhesion* regime while retracting from the surface which result in an attractive force and adhesion neck.

IV. Decoupling AFM Micro/Nanoforces

Using the results of the collision detection, namely the indentation depth and the normal direction of the contact between tip and sample surface, the two force signals from the AFM, one for lateral forces and one for normal and frontal forces, can be decomposed into 3D. Using a simple model for bending behavior of the AFM probe, the force exerted on the tip can then be determined in 3D by geometric considerations.

A. AFM Probe Model

The probe of the AFM consists of a cantilever beam with a parabolic tip at its end (here, this parabolic tip is approximated as a sphere). For the case of a rectangular cross-sectioned cantilever, the relation between forces exerted on the tip and the tip's deflection from its position at zero force can be obtained by stating the Bernoulli-Euler equation and integrating twice, which first yields the slopes of the deformed beam and then its deflections. Evaluating the normal z-axis and lateral y-axis deflections and torsional deflection caused by y-axis lateral force, the following model is obtained (Figure 1) [6,19]:

$$\Delta\mathbf{X} = \begin{bmatrix}\Delta x\\ \Delta y\\ \Delta z\end{bmatrix} = \begin{bmatrix}1/k_x & 0 & 1/k_{xz}\\ 0 & 1/k_{y,b}+1/k_{y,t} & 0\\ 1/k_{xz} & 0 & 1/k_z\end{bmatrix}\begin{bmatrix}F_x\\ F_y\\ F_z\end{bmatrix} \tag{3}$$

with the following stiffness variables, expressed in terms of Young's modulus E, width w, thickness t, length l, tip height h, and Poisson ratio ν of the AFM probe:

$$k_z = \frac{Ewt^3}{4l^3},\quad k_x = \frac{l^2}{3h^2}k_z,\quad k_{xz} = \frac{2l}{3h}k_z,$$
$$k_{y,b} = \left(\frac{w}{t}\right)^2 k_z,\quad k_{y,t} = \frac{2l^2}{3h^2(1+\nu)}k_z. \tag{4}$$

The force in lateral y-direction cause both lateral and torsional bending of the cantilever beam. The optical lever method however only measures angular twisting of the beam, which in case of torsion without bending is directly proportional to the exerted force. Therefore, wide and thin cantilevers for which lateral bending can be neglected are selected here. Lateral forces can therefore be determined directly as the resulting torsion angle $\Delta\theta$ can be approximated by the following expression [19]:

$$\Delta\theta = \frac{lhF_y}{\beta G w t^3} = \frac{1}{3h\beta}\frac{F_y}{k_{y,t}} \tag{5}$$

where $\beta=t/w$ is a geometry-dependent constant and G is the shear modulus of the beam material.

Forces in normal (z-axis) and frontal (x-axis) direction both cause equally directed changes in angular orientation of the beam's end. Therefore their measurement obtained by the optical lever method, is coupled. As the angular change $\Delta\alpha$ is very small, it can be approximated by the slope at the end of the beam $z'(l)=\tan(\alpha)$, which yields:

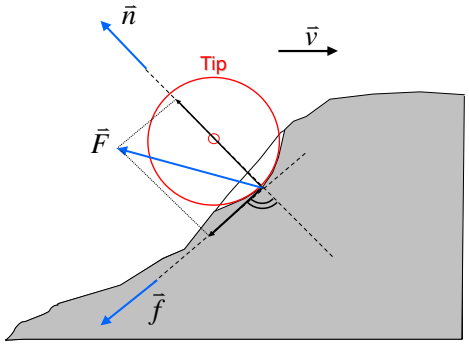

Figure 5. Geometry of the tip-sample contact.

$$\Delta\alpha = \frac{l^2}{2EI}\left[F_z + \frac{2a}{l}F_x\right]. \tag{6}$$

where $I=wh^3/12$ is the beam's flexure momentum of inertia referred to the y-axis.

For a force in either x- or z-direction, there is a one-to-one correspondence between tilt angle α at the end of the beam and the acting force. For a force composed of both, components in x- and z-directions, this one-to-one correspondence is no longer valid. This means that while lateral forces can be determined directly, frontal and normal forces cannot be measured separately and the overall direction of the force exerted on the tip cannot be obtained from the AFM alone.

B. Blending Modeled Contact Geometry and Force Measurement

The information obtained from the AFM is the changes in angular orientation of the beam's end $\Delta\theta$ caused by lateral forces on the one hand and $\Delta\alpha$ caused by frontal and normal forces on the other hand. The desired information are two vectors $\boldsymbol{F}^T=(F_x,F_y,F_z)$ and $\boldsymbol{x}^T=(x_x,x_y,x_z)$, describing the overall force acting on the tip and the deflection of the tip from its position at zero force, respectively. As discussed, the measured torsion angle $\Delta\theta$ and the lateral force F_y are directly proportional for thin wide cantilevers. Thus, in lateral direction, all necessary information is known and can be determined directly from (5). However, neither F_x nor F_z can be determined directly from measured angular change. Yet with a simple geometric consideration, one more relation for the components of the overall force vector $\boldsymbol{F}$ can be obtained.

As can be seen in Figure 5, it is obvious that $\boldsymbol{F}$, consisting of a force component normal to the surface and a friction component tangential to it, has to be in the plane defined by $\boldsymbol{n}$ and $\boldsymbol{f}$. The direction of the friction force is opposed to the tip movement represented by $\boldsymbol{v}$ and tangential to the surface at the contact point. Letting $\boldsymbol{v}^T=(v_x,v_y,v_z)$, $\boldsymbol{f}$ can be written as $\boldsymbol{f}^T=(-v_x,-v_y,f_z)$ where

$$\vec{f}\circ\vec{n} = 0 \Rightarrow f_z = -\frac{v_x n_x + v_y n_y}{n_z} \tag{7}$$

This equation assumes a surface topography with no perpendicular inclinations (which would mean $n_z=0$) which is

realistic since AFM scans with a parabolic tip can not image side-walls (only carbon nanotube tip attached high aspect ratio AFM probe tips can image this type of side-walls).

Now, the vector $\boldsymbol{p}=(\boldsymbol{n}\times\boldsymbol{f})$, which is perpendicular to the plane the overall force is in, can be computed. $\boldsymbol{F}$ and $\boldsymbol{p}$ are perpendicular such that

$$\vec{F} \circ \vec{p} = F_x p_x + F_y p_y + F_z p_z = 0 \ . \tag{8}$$

Combining (6) and (8) yields:

$$F_x = \frac{\frac{p_y}{p_z} F_y + \frac{2EI\Delta\alpha}{l^2}}{\frac{2a}{l} - \frac{p_x}{p_z}} \qquad F_z = \frac{\frac{p_y}{p_x} F_y + \frac{EI\Delta\alpha}{la}}{\frac{l}{2a} - \frac{p_z}{p_x}} \tag{9}$$

This calculation is used when the tip moves in contact with the surface in x-y-z plane and all (F_x,F_y,F_z) force components and (p_x, p_y, p_z) are non-zero. If the tip moves in x-z or z-plane only while in contact with the surface, then $p_x=p_z=0$ or $p_x=p_y=p_z=0$, respectively which causes singularity in (9). Therefore, for the z-plane motion case, $F_x=F_y=0$ is taken, and F_z is calculated only using the Maugis-Dugdale elastic deformation model in z-direction as shown in Figure 4. For the x-z plane motion case, z-deflection Δz is a function of both F_x and F_z from (3) as

$$\Delta z = \frac{1}{k_z}\left(\frac{3h}{2l} F_x + F_z\right) . \tag{10}$$

Then, to compute F_x and F_z separately, a micro/nanoscale friction model is required which could be given as [20]

$$F_x = \mu F_z + \tau A \ . \tag{11}$$

where μ and τ are the friction coefficient and shear stress between the tip and surface, respectively, and A is the contact area which is a function of the vertical load F_z, interfacial surface energy, and equivalent modulus of elasticity between the tip and surfaces materials [3]. Here, assuming the normal load based friction is relatively much higher than the adhesion dominated friction, we can take $F_x=\mu F_z$ which results in

$$F_z = \frac{k_z \Delta z}{1 + \frac{3h\mu}{2l}} \qquad F_x = \mu F_z \ . \tag{12}$$

Using only the angular orientations $(\Delta\theta, \Delta\alpha)$ measured by the AFM and the geometric information obtained from the collision detection algorithm, the force exerted on the tip can be resolved in all possible cases using (9) and (12). Having determined the force vector, also the tip's deflection from its position at zero force can be obtained. This way, decoupled 3D force feedback can be given to the user and the tip deflection can be used in the control scheme to compensate for the compliance of the probing tool and to allow direct position control of the AFM tip, not only of the compliant cantilever's base.

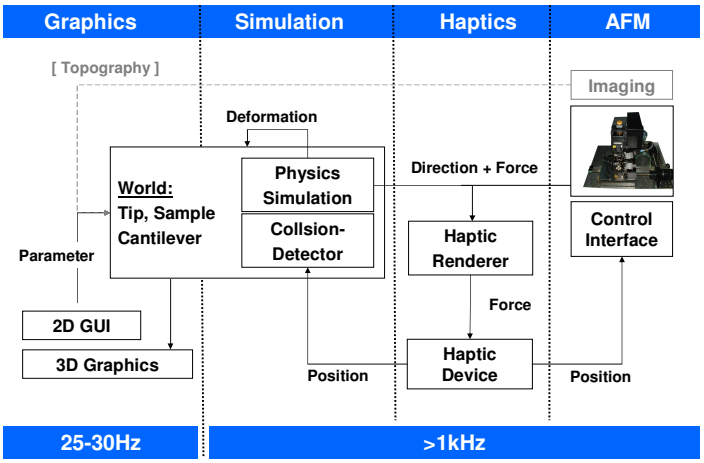

Figure 6. Augmented reality system overview.

V. System Setup

The implemented system as illustrated in Figure 6 comprises a 3D computer graphics interface based upon OpenGL, a real-time nanomechanics simulation of the tip-sample contact behavior, and a Phantom® Premium 1.5T model haptic interface. Here, AFM system is currently just simulated using real AFM images and micro/nano-physics simulations and using a real AFM system with real nanoforce measurements is a future work. Figure 7 displays the visual and haptic user interface setup. The system was designed in a multithreaded way: while graphics are updated at a rate of approximately 25 Hz, the simulation, haptic control, and the AFM control are updated at a rate well above 1 kHz. The details of the graphical user interface are displayed in Figure 8. In this interface, real-time 3D surface deformation, AFM tip position, and nanoforces on the AFM tip in a zoomed area, 3D AFM image of the scanned real surface, AFM cantilever deflection, and on-line 3D force and position data are displayed.

At the current status, the system is implemented as a simulation environment, in which AFM online control is not yet integrated, but the behavior of the real AFM is simulated. However, the system is designed in a manner that any commercial AFM with a low-level control interface can be integrated modularly. The system can currently be used as experimental environment for haptic exploration of previously scanned AFM images and for experimental evaluation of the augmented reality user interface quality.

VI. Experiments

To test the accuracy, usability, and reliability of the proposed user interface system with simulated nanomechanics, a set of experiments is designed using the setup given in Section V. The below is an overview of the different components of the experiments.

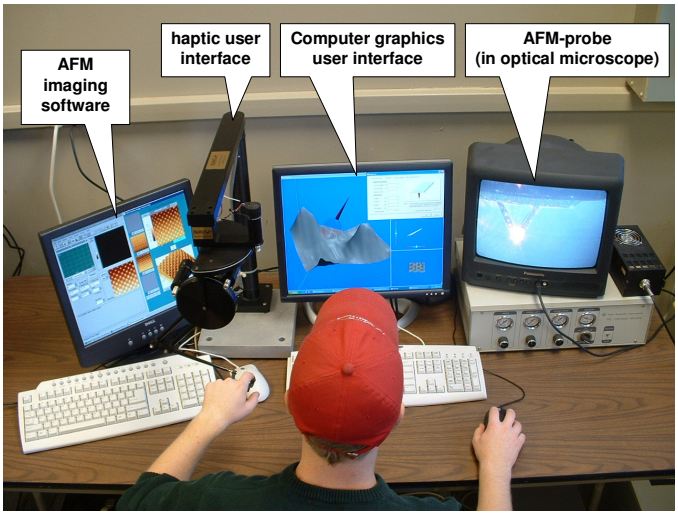

Figure 7. The photo of the visual and haptic user interface setup.

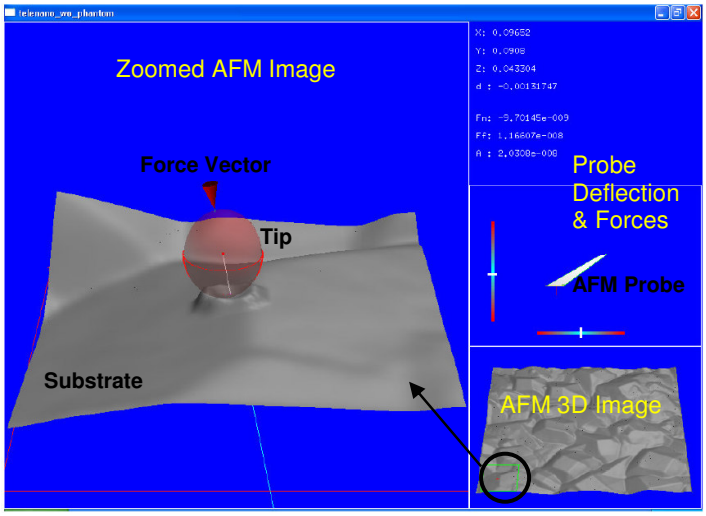

Figure 8. Snapshot of the implemented graphical user interface: left window shows the 3D real-time probe tip, zoomed AFM image of the surface, and nanoforces; right-bottom window displays the overall 3D AFM surface topography; right-middle window displays the AFM cantilever deflections; right-top window shows the real-time data of 3D forces and AFM tip position.

A. *Tasks*

Experiment is made up of three tasks. Each involves positioning the probe in a pre-defined position on, above, or below the surface (Figure 9). Each task has its own set of challenges, given that our models accurately approximate the nanophysical properties of the surface. Task A is expected to be the most difficult to achieve. Since Task A requires positioning the probe at such a small distance above the surface, nonlinear non-contact forces pulling the probe towards the surface may prevent the probe from being held at that distance. However, this is a crucial task to consider since many applications, such as manipulating carbon nanotubes and nanoparticles with direct friction measurement, require holding the probe up close to but not touching the surface. Task B involves the positioning of the AFM tip on the surface for 3D topography following with minimal deformation. Task C aims to position the tip below surface by indenting it elastically to get surface compliance feedback or plastically deform it for nanomanipulation applications. For a silicon tip, Task C may not be applicable to surfaces that are very stiff, such as glass.

B. *Constants*

For all tasks, user interface system consisting of the visual and haptic feedback was kept the same. In addition, in order to decrease the complexity, experiments were performed on a locally flat surface. The tip size of our AFM tip radius was kept at 15 nm (which is the standard tip size for most commercially available AFMs). Finally, the probe stiffness was taken high (14 N/m). This is preferable for two reasons. First, since a stiff probe applies more force on the surface, it is more responsive to topographical change. In addition, a soft probe would easily be subjected to the attractive nature of the non-contact forces. This makes it difficult to perform tasks that require the probe to be above the surface (such as Task A from Figure 9) since the probe could jump-into-contact easily which is undesirable. Thus, high probe stiffness allows us to perform experiments on a larger variety of surfaces.

TABLE 1 MATERIAL PROPERTY OF THE TESTED SURFACES

Material	*Young's Modulus (GPa)*	*Adhesion (J/m^2)*	*Poisson Ratio*
Silicon Oxide	70	0.2	0.27
Polystyrene	2	0.066	0.4
Silicon Rubber	0.001	0.022	0.5

C. *Physical Parameters*

There are three parameters that we varied in our experiments. One is the Young's modulus which represents the hardness of the material or surface. Second is the adhesion or surface energy of the surface; this factor determines how sticky the surface is. Finally, the Poisson ratio is a ratio of the transverse strain to the normal strain of the material. We will use three different types of material ranging from a hard surface (glass) to a soft surface (rubber) each having its own set of values for the parameters given in Table 1.

D. *Method*

At the beginning of the experiment, each user was briefly introduced to the system. They had about five minutes to

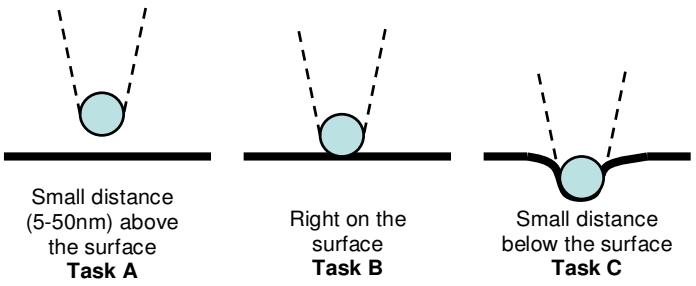

Figure 9. Experiment tasks (the sphere represents the AFM tip).

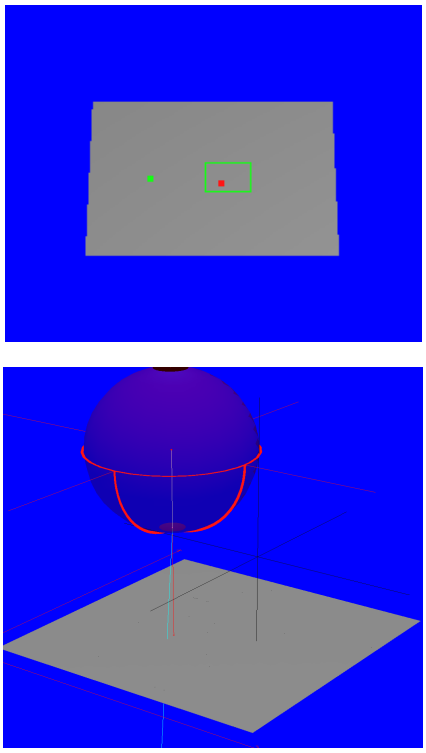

Figure 10. a) Global view of target position (in green) b) Detailed view of target position (black crosshair).

familiarize themselves with the haptic device as well as the visual interface. Afterwards, they began the experiment. For each task, the user's probe position would start approximately in the middle of the surface. They then had to use the global view (Figure 10a) to locate the target (in green), and move towards the target. The goal is to position the probe as close to the target position as possible. The target in the interface is depicted by a three dimensional crosshair (Figure 10b); its center is considered the target position. Hence, the error is measured from this point to the probe's center.

For each task, the user would press a button to begin, and the same button again when they feel that they have positioned the probe as accurately as possible. Directional buttons allowed the user to rotate the view vertically and horizontally along the plane. After each target acquisition, the material properties would be changed, and the procedure repeated. Each task is performed with all three materials, with the exception of the third task. The third task omits the first material (silicon oxide) since the third task requires deforming the surface; elastic deformation is very tiny for hard surfaces. Finally, each task is repeated two more times. A total of 162 data points were collected for six different users.

E. Evaluation

Positioning error and average time is calculated for each task and material. If our nanophysical and geometry models are accurate, Task A should produce the highest percent error since it is the hardest task to achieve given the nature of the task. Also, Task C should be more difficult with Silicon Rubber than Polystyrene. The softness of Silicon Rubber will

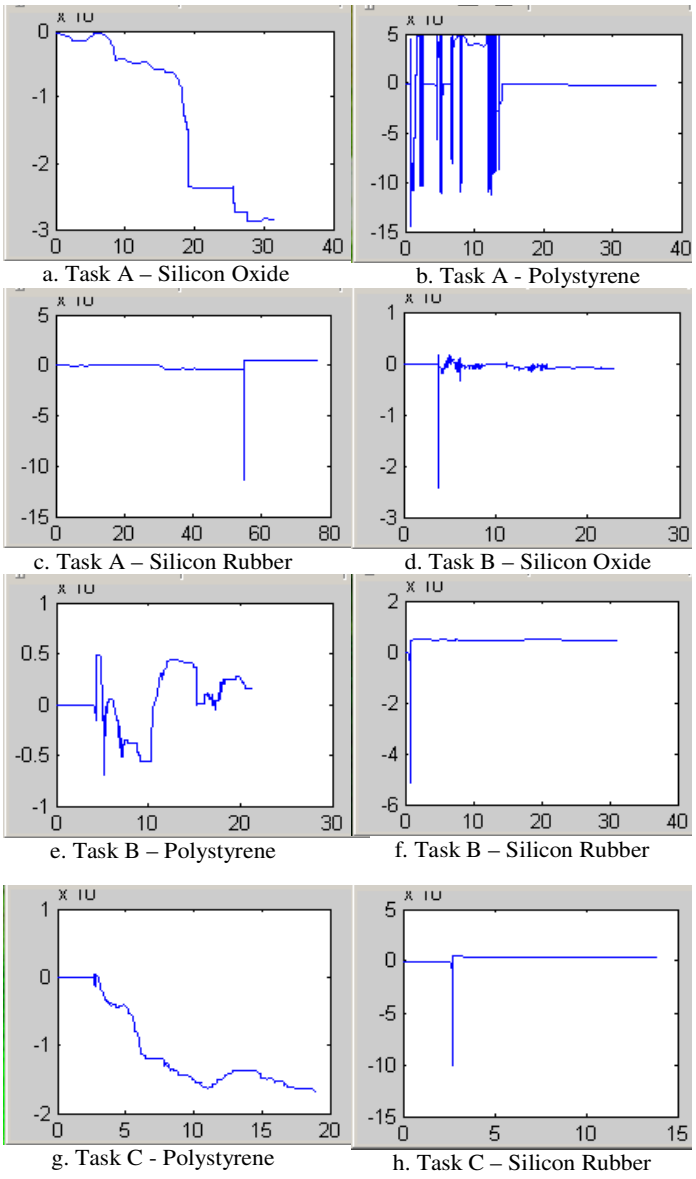

Figure 11. Sample force ($x10^{-7}$ *N*) vs. time (*sec*) experimental plots for each task and material.

give the user less force feedback, which facilitates overshooting the deformation position. In addition, user's performance should improve with the number of trials since it is expected that they will need some time to become familiar with the interface. For analysis purposes, trajectories and forces are also recorded.

F. Analysis

Before any experiments were conducted, one untrained user was put through certain parts of the experiment and asked for feedback. This was used to make quick improvements to the experimental setup. With the exception of one user, all further experiments were performed with untrained users. For these users, this was their first time using the interface. Data related to the positioning error as well as the time required to complete each task was collected for each task and each material.

VII. Results

This section shows the test results and discusses its implications. Among the untrained users, it was expected that the percent error would decrease with the trials. We expected the user to become more and more familiarized with the interface and hence, make more accurate target acquisitions. This was not the case however. In fact, we found no correlation between the number of trials and the accuracy of the results. Sample force vs. time experimental data for a given user is shown in Figure 11. Also, we expected Task A to be the most difficult, and anticipated that it would have the highest percent error. Based on our data (Figure 12), Task B had the highest average percent error, followed by Task C and then Task A. The difficulties in terms of materials are fairly even for Task A. Silicon Oxide made Task B more difficult than Silicon Rubber. Task C was much more difficult in Silicon Rubber than Polystyrene.

As for time, we expected the time required to perform each task to decrease with the trials (Figure 13). This was also not the case. In addition, it was expected that if the average time was longer, then the percent error should be less. This is because the user would be taking more time to perform the task, hence making fewer accuracy errors. With the exception of Task C, no correlation was found between how accurate a user was, to the average time required to complete the task. The faster users did not necessary have a higher average error and likewise, the slower users did not necessarily have a lower average error. For Task C however, the average time required to complete the task for Polystyrene is much higher than more Silicon Rubber (Figure 13). Consequently, the average error is much less for Polystyrene than for Silicon Rubber.

VIII. Discussion

Although Task A (positioning the probe slightly above the surface) seemed like the hardest task, most users did not have much difficulty completing it. It seemed manageable, especially if the user made contact with the surface first. Using this strategy, the user did not have to feel the nonlinear forces, since they were already making contact with the surface. Hence, they simply had to apply a force to counter the contact forces, which are much more stable than the nonlinear forces. This strategy was not as successful for Silicon Oxide. Silicon Oxide has a higher Young's modulus. Since it is a harder material, the probe does not stay in contact with the surface as long as for softer materials when pulling up from the surface. Users who made contact with this type of surface had to first apply a force to disengage from the surface in order to reach the target position. The extra force caused the user to go beyond the target, requiring them to then reposition.

Task B (positioning right on the surface) was the most challenging. Most users wanted to position the probe slightly above the surface, instead of on the surface itself. Therefore, they were constantly fighting the nonlinear forces. These forces caused the haptic device to oscillate, making if difficult for the user to hold it still. In essence, this task unexpectedly represented the difficulties of what we initially predicted Task A would represent.

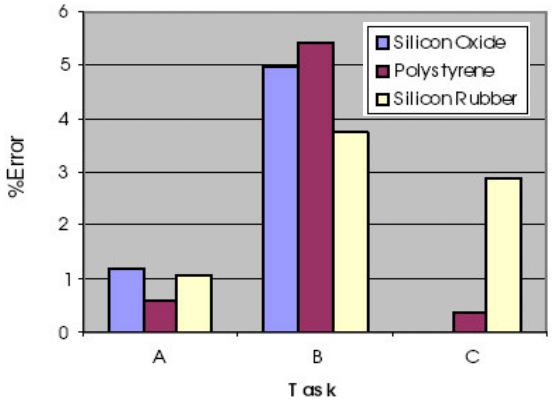

Figure 12. Comparing the average percentage positioning error for each task and material.

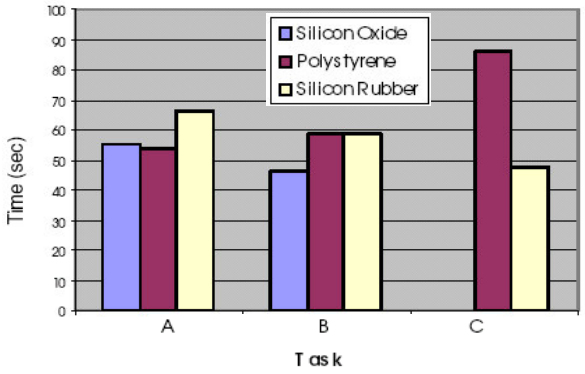

Figure 13. Comparing the average completion time for each task and material.

As predicted by our models, Task C (positioning below the surface) had a higher percent error for Silicon Rubber than Polystyrene. The softness of Silicon Rubber resulted in less normal force feedback (Figure 11c, 11f, and 11h); this made it easier for users to unnoticeably push too far into the surface, surpassing the target position.

The average time required for each task did not vary based on the number of trials. Depending on the trial, some users encountered more difficulties with one trial than with another trial of the same task and material. This was caused by unexpected interactions that took place during the trial. For example, for Task A on one trial, the user might easily move to the target position without any complications. For another trial, however, they may accidentally make contact with the surface; therefore, they will have to adjust the probe, taking more time. As a result of these random interactions, the time required to complete each task does not necessarily decrease with each trial as predicted. By the same reasoning, it is also not necessarily true that the more time spent on a trial the more accurate the trial.

These results suggest that many challenges exist in the nanoscale world which needs to be validated with real AFM experiments. Despite these challenges, with some training, it is possible to achieve good accuracy and smooth trajectories.

IX. Conclusion

Using real-time simulations to gain additional information, which cannot be obtained from an AFM directly, is an effective way to enrich the intuitiveness of AFM-based

telenanorobotics without the need to introduce new visual sensing methods. Using the models proposed in this paper and blending their results with the measurements sensed by the AFM, surface deformations are visualized in real-time and the user can be given heretofore impossible 3D feedback. The geometry of the contact between tip and sample surface is simulated in a fast and efficient model, assuming a sphere-based probe in contact with an arbitrarily shaped surface. Testing the proposed user interface for three tasks of positioning the AFM tip above on a surface gave new insights about the difficulties and errors in the user interface due to non-contact and contact nanoforces.

The implemented user interface works well in simulated mode, while it remains to be shown in experiments that simulations and AFM can be matched closely sufficient. As future work, real-time AFM based nanomanipulation applications such as nanoparticle and carbon nanotube pushing and polymer nanofiber pulling using the proposed AR user interface for animated real-time visualization of the AFM tip and nanoobjects will be demonstrated. Here, also nanomanipulation mechanics will be integrated to the current nanomechanics models for also animating the nanoobject motion and behavior.

ACKNOWLEDGMENT

This work was supported by NSF CAREER award program (NSF IIS-0448042).

REFERENCES

[1] Hollis, R., Salcudeau, S., and Abraham, D. W., "Toward a Tele-Nanorobotic Manipulation System with Atomic Scale Force Feedback and Motion Resolution", *Proc. of IEEE Micro Electro Mechanical Systems*, pp. 203-208, 1990.

[2] Sitti, M., "Teleoperated 2-D Micro/Nanomanipulation using an Atomic Force Microscope, *Ph.D. Thesis*, Dept. of Electrical Engineering, University of Tokyo, Tokyo, Japan, 1999.

[3] Sitti, M. and Hashimoto, H., "Teleoperated Touch Feedback from Surfaces at the Nanoscale: Modeling and Experiments", *IEEE/ASME Transaction on Mechatronics*, vol. 8, no. 2, pp. 287-298, 2003.

[4] Kim, D.-H., Park J., Kim, B., and Kim, K., "Modeling and Simulation of Nanorobotic Manipulation with an AFM probe", *Proc. of the Int. Conference on Control, Automation and Systems*, 2002.

[5] Li, G., Xi, N., Yu, M., Salem, F., Wang, D., and Li, J., "Manipulation of Living Cells by Atomic Force Microscopy," *Proc. of IEEE/ASME International Conference on Advanced Intelligent Mechatronics*, pp. 862-867, 2003.

[6] Sitti, M., Aruk, B., Shintani, H., and Hashimoto, H., "Scaled Teleoperation System for Nano Scale Interaction and Manipulation", *Advanced Robotics Journal*, vol. 17, no. 3, pp. 275-291, 2003.

[7] Baur, C., Grange, S., Conti, F., and Helmer, P., "The Delta haptic Device as Nanomanipulator", *Proc. of SPIE Microrobotics and Microassembly III*, 2001.

[8] Rubio-Sierra, F. J., Stark, R. W., Talhammer, S., and Heckl, W. M., "Force-feedback joystick as a low cost haptic interface for an atomic force microscopy nanomanipulator, *Applied Physics A*, vol. 76, pp. 903-906, 2003.

[9] Taylor, R.M., II, Robinett, W., Chi, V.L., Brooks, F.P., Wright, W.V., Williams, R.S., and Snyder, E.J., "The Nanomanipulator: a virtual-reality interface for a scanning tunneling microscope," *Proc. of the SIGGRAPH*, pp. 127-134, 1993.

[10] Resch, R., Baur, C., Bugacov, A., Koel, B. E., Madhukar, A., Requicha, A. A. G., and Will, P., "Building and manipulating 3-D and linked 2-D structures of nanoparticles using scanning force microscopy", *Langmuir*, vol. 14, no. 23, pp. 6613-6616, November 1998.

[11] Junno, T., Deppert, K., Montelius, L., and Samuelson, L., "Controlled Manipulation of Nanoparticles with an Atomic Force Microscope", *Appl. Physics Letters*, vol. 66, pp. 3627-3629, June 1995.

[12] Sitti, M. and Hashimoto, H., "Controlled Pushing of Nanoparticles: Modeling and Experiments", *IEEE/ASME Trans. on Mechatronics*, vol. 5, pp. 199-211, 2000.

[13] Talhammer, S. and Stark, R. W., "The AFM as a tool for chromosomal dissection – the influence of physical parameters", *Applied Physics A*, vol. 66, pp. 579-584, 1998.

[14] Falvo, M., Taylor II, R. M., Helser, A., Chi, V., Brooks Jr., F. P., Washburn, S., and Superfine, R. "Rolling and Sliding on the Nanometer Scale," January 21, *Nature*, vol. 397, pp. 236-238, 1999.

[15] Taylor, R.M. II and Superfine, R., "Advanced Interfaces to Scanned-Probe Microscopes" in Handbook of Nanostructured Materials and Nanotechnology, Hari Singh Nalwa (Ed.), Academic Press, 2000.

[16] Hatamura, Y. and Morishita, H., "Direct Coupling System between Nanometer World and Human World", *Proc of. IEEE Micro Electro Mechanical Systems*, pp. 203-208, 1990.

[17] Corso, J., Chhungani, J., and Okamura, A. M., "Interactive Haptic Rendering of Deformable Surfaces Based on the Medial Axis Transform", *Proc of. Eurohaptics*, pp. 92-98, 2002.

[18] Piegl, L. and Tiller, W., *The NURBS Book*, Springer Verlag, Berlin: 1995.

[19] Marti, O., "AFM Instrumentation and tips", *Handbook of micro/nano-tribology*, 2nd ed., Bhushan B. (Ed.), CRC Press, Washington D.C., 1999.

[20] Sitti, M., "Nanotribological characterization system by AFM probe based controlled pushing," *IEEE/ASME Trans. on Mechatronics*, vol. 9, no. 2, pp. 343-349, June 2004.

Wolfgang Vogl received a MSc (diploma) degree in Mechanical Engineering from the Technical University Munich, Germany in 2003. He conducted his master thesis at the Nanorobotics Laboratory at Carnegie Mellon University, Pittsburgh, PA where he worked on advanced user interfaces for teleoperated nanomanipulation using atomic force microscopes. He is currently pursuing his PhD studies at the Technical University Munich, Germany where his research interests include advanced man-machine interfaces, computer vision, and augmented and virtual reality applications in industrial scenarios.

Bernice Ma received the BSc degree in Computer Science from Carnegie Mellon University in 2004. Her research interests include human-machine interfaces, Augmented Reality, and computer graphics.

Metin Sitti (S'94-M'00) received the BSc and MSc degrees in Electrical and Electronic Engineering from Bogazici University, Istanbul, Turkey, in 1992 and 1994, respectively, and the PhD degree in Electrical Engineering from the University of Tokyo, Tokyo, Japan, in 1999. He worked in the CAD/CAM Robotics Department in the TUBITAK Marmara Research Center, Kocaeli, Turkey, as a research engineer during 1994-1996, working on visual servoing, computer vision, and robot control projects. He was a recipient of the Monbusho Research Fellowship during his PhD study in Japan. He was a research scientist and lecturer at the Department of Electrical Engineering and Computer Sciences, University of California at Berkeley during 1999-2002. He is currently an assistant professor at the Mechanical Engineering Department and the Robotics Institute, Carnegie Mellon University, Pittsburgh, PA. His research interests include micro/nanomanipulation, miniature microrobotics, biologically inspired micro/nanosystems, and advanced human-machine interfaces.

He received the NSF CAREER award in 2005 for his nanorobotics related research and teaching activities and the Struminger award for teaching

activities at Carnegie Mellon. He is elected as the Distinguished Lecturer for the IEEE Robotics and Automation Society for 2006-2007. He received the best paper award in the IEEE/RSJ International Conference on Intelligent Robots and Systems in 1998, the best video award in the IEEE Robotics and Automation Conference in 2002, and the best biomimetics paper award in the IEEE Robotics and Biomimetics Conference in 2004. He is the chair of the Technical Committee on Nanorobotics and Nanomanufacturing in the IEEE Nanotechnology Council and the Technical Committee on Prototyping in Robotics and Automation in the IEEE Robotics and Automation Society, and a member of IEEE, ASME, and Robotics Society of Japan.